IJMMM International Journal of Minerals, Metallurgy and Materials 矿物冶金与材料学报（英文版）

Kinetic analysis of iron ore powder reaction with hydrogen–carbon monoxide

Xudong Mao, Pritesh Garg, Xiaojun Hu, Yuan Li, Samik Nag, Saurabh Kundu, and Jianliang Zhang

Cite this article as:
Xudong Mao, Pritesh Garg, Xiaojun Hu, Yuan Li, Samik Nag, Saurabh Kundu, and Jianliang Zhang, Kinetic analysis of iron ore powder reaction with hydrogen–carbon monoxide, *Int. J. Miner. Metall. Mater.*, 29(2022), No. 10, pp. 1882-1890. https://doi.org/10.1007/s12613-022-2512-6

View the article online at SpringerLink or IJMMM Webpage.

International Journal of Minerals, Metallurgy and Materials
Volume 29, Number 10, October 2022, Page 1882
https://doi.org/10.1007/s12613-022-2512-6

Kinetic analysis of iron ore powder reaction with hydrogen–carbon monoxide

Xudong Mao[1)], *Pritesh Garg*[2)], *Xiaojun Hu*[1),✉], *Yuan Li*[1)], *Samik Nag*[2)], *Saurabh Kundu*[2)], *and Jianliang Zhang*[3)]

1) State Key Laboratory of Advanced Metallurgy, University of Science and Technology Beijing, Beijing 100083, China
2) R&D, Tata Steel Ltd., Jamshedpur, Jharkhand 831001, India
3) School of Metallurgical and Ecological Engineering, University of Science and Technology Beijing, Beijing 100083, China
(Received: 11 November 2021; revised: 27 April 2022; accepted: 29 April 2022)

Abstract: Iron ore powder was isothermally reduced at 1023–1373 K with hydrogen/carbon monoxide gas mixture (from 0vol%H_2/100vol%CO to 100vol%H_2/0vol%CO). Results indicated that the whole reduction process could be divided into two parts that proceed in series. The first part represents a double-step reduction (Fe_2O_3→Fe_3O_4→FeO), in which the kinetic condition is more feasible compared with that in the second part representing a single-step reduction (FeO→Fe). The influence of hydrogen partial pressure on the reduction rate gradually increases as the reaction proceeds. The average reduction rate of hematite ore with pure hydrogen is about three and four times higher than that with pure carbon monoxide at 1173 and 1373 K, respectively. In addition, the logarithm of the average rate is linear to the composition of the gas mixture. Hydrogen can prominently promote carbon deposition to about 30% at 1023 K. The apparent activation energy of the reduction stage increases from about 35.0 to 45.4 kJ/mol with the increase in hydrogen content from 20vol% to 100vol%. This finding reveals that the possible rate-controlling step at this stage is the combined gas diffusion and interfacial chemical reaction.

Keywords: reduction; carbon monoxide; hydrogen; kinetics; mechanism

1. Introduction

Blast furnace ironmaking remains the mainstream ironmaking process in the world and inevitably brings billions of tons of carbon dioxide emissions [1–2]. Excessive emissions of carbon dioxide further aggravate the global greenhouse effect; therefore, a series of measures must be carried out to reduce carbon dioxide emissions. Hydrogen substitution for coke in iron production shows excellent superiority. In terms of environmental protection, the use of hydrogen to produce iron can avoid many carbon emissions. Owing to the smaller molecular size of hydrogen than carbon monoxide, the former can efficiently diffuse to the reaction interface to speed up the reduction rate. In some parts of the world, the efficient use of hydrogen in the ironmaking industry has gradually been promoted [3]. Therefore, further research is necessary for iron ore reduction by hydrogen under blast furnace conditions.

If only a part of the carbon raw material is replaced by hydrogen in the reactor, then the competitive reduction of iron oxide by hydrogen/carbon monoxide gas mixture will inevitably occur. Kim *et al.* [4] studied the retardation kinetics of cylindrical compacts of magnetite reduction and found that the presence or absence of retardation had a huge relationship with the reaction conditions. Researchers [5–6] proposed a novel kinetics model and revealed the reduction mechanism of metal oxides by hydrogen under external gas diffusion as the controlling condition. El-Geassy *et al.* [7] considered that the particle size of iron ore should not be as small as possible. Sun *et al.* [8] studied coke gasification kinetics in the CO_2/CO/H_2/H_2O/N_2 system under industrial blast furnace conditions and considered that the choice of kinetics model (Random Pore Model, Volumetric Model, and Grain Model) does not have a substantial effect on the description of coke gasification mechanism. Tahari *et al.* [9] claimed that CO was a faster reducer at low reduction temperature than H_2, which remained a good reducing agent in competing reduction. On the contrary, Rodriguez *et al.* [10] investigated the reduction kinetics of hematite compacts by a H_2/CO gas mixture at 823 to 923 K and proposed that the reduction rate increased with the H_2 content in the gas mixture. Bonalde *et al.* [11] studied the kinetics of iron oxide reduction at 1023 K with hydrogen and carbon monoxide and observed that the reaction control type was mixed control as hydrogen and carbon monoxide were applied as reducing agents, respectively. Steinfeld *et al.* [12] used a H_2/H_2O/CH_4/CO/CO_2 gas mixture to reduce iron oxides and found that carbon deposition occurred below 1273 K and at low hydrogen concentrations. However, Towhidi and Szekely [13] researched hematite pellet reduction in the temperature range from 873 to 1507 K with H_2/CO/N_2 gas mixture and observed that carbon deposition cannot occur when the temperature is higher than 1173

✉ Corresponding author: Xiaojun Hu E-mail: huxiaojun@ustb.edu.cn

K. A disagreement arose concerning some details of iron ore reduction using a hydrogen/carbon monoxide gas mixture. Therefore, an in-depth study on iron ore reduction by hydrogen/carbon monoxide gas mixture is necessary.

The kinetics of iron ore reduction by hydrogen-containing water vapor has been studied in our previous work [14]. In the present research, the reduction kinetics of iron ore at different reduction temperatures and different compositions of reducing agents was further studied, and the reduction behavior in each situation was specified. Meanwhile, a semi-empirical formula to determine the relationship between the average rate of reduction and the composition of reducing gas under certain conditions was obtained by assuming the model conditions and combining the experimental results. This formula could be used to help understand the reduction situation at different locations in the reactor and make further improvements.

2. Experimental

2.1. Sample preparation

Iron ore pellets (green concentrate rich in hematite) with Fe_2O_3 content of 86wt% were provided by a major steel company in India and crushed into powder with an average particle size of ~200 mesh (74 μm). Particle size distribution was analyzed by a laser particle size analyzer (CLF-2, Malvern) and is given in Fig.1. The phase and chemical composition of hematite ore were identified by X-ray diffraction (XRD, SmartLab, Rigaku) and X-ray fluorescence (XRF, EDX-8000, Shimadzu), respectively. Given the relatively small proportion of other components in hematite ore, as shown in Table 1, the XRD results indicated the low characteristic peak of the gangue phase. The hematite ore powder was stored in a high-temperature vacuum drying oven and dehydrated for at least 48 h before the experiment. The microstructure of hematite ore powder in Fig. 2 indicated the lack of cracks and holes on the sample surface before the reaction.

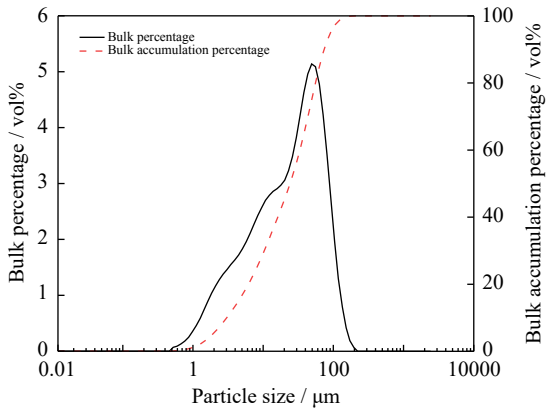

Fig. 1. Particle size distribution of hematite ore powder.

Table 1. Main components of hematite ore wt%

Fe_2O_3	Al_2O_3	SiO_2	CaO	MgO
86.00	3.70	5.67	1.45	2.55

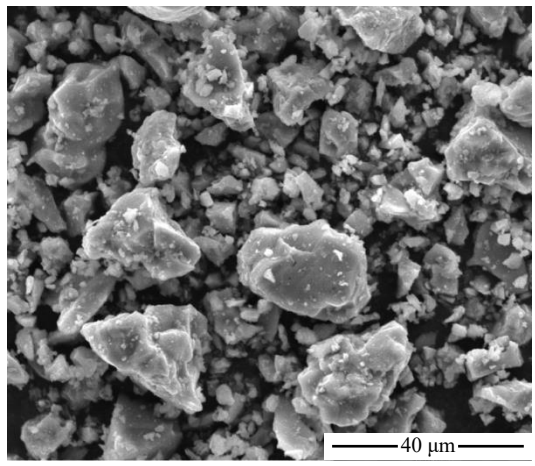

Fig. 2. Microstructure of the hematite ore powder.

2.2. Experimental apparatus and procedure

The experiment was carried out using a thermo-gravimetric analyzer (TGA, HCT-4, Henven) with a precision of ±1 μg, and the mass loss was recorded at 1 Hz. Alumina crucibles with 16 mm inner diameter were cleaned by an ultrasonic cleaner and then dried in a vacuum drying oven before use. The hematite ore was isothermally reduced with hydrogen/carbon monoxide gas mixture at 1023–1373 K. In brief, 100 mg of hematite ore sample was placed in the TGA and heated to the desired temperature under an argon atmosphere (purity of 99.999%) with a gas flow rate of 40 mL/min controlled by the American Alicat mass flowmeter with an accuracy of ±0.5%. When the temperature was reached, the argon was switched to the hydrogen/carbon monoxide gas mixture. A schematic of the experimental apparatus is given in Fig. 3.

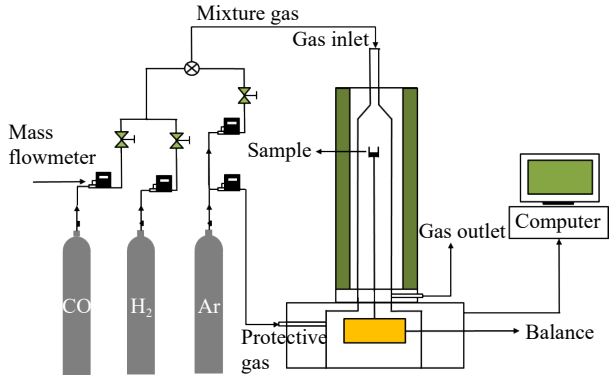

Fig. 3. Schematic of the experimental setup.

After the reduction, the hydrogen/carbon monoxide gas mixture was switched to argon, and the sample was cooled to room temperature. The weight of the hematite ore sample was continuously measured by the TGA. The different phases and the structure of the reduction product were characterized by XRD and scanning electron microscope (SEM, MLA250, FEI).

2.3. Principle of reduction

In general, hydrogen and carbon monoxide can reduce hematite to metallic iron, but their reduction behaviors vary

due to their different physical and chemical properties. Hydrogen can rapidly reduce hematite to iron due to its small size and strong reducing ability. For hematite reduction to iron using carbon monoxide, carbon deposition might occur under certain conditions. Given that carbon deposition is accompanied by an exothermic effect, this reaction will be weakened with the increase in experimental temperature. Carbon deposition no longer occurs when the experimental temperature exceeds the transition temperature of thermodynamic theory. If hydrogen is added to carbon monoxide to reduce hematite, then the reduction rate of hematite and the deposition rate of carbon will be converted. Under the experimental conditions of carbon formation, the whole reaction can be divided into two parts. In the first part of the reaction, hematite is reduced to metallic iron by the stepwise reaction. In the second part, carbon monoxide is catalyzed by iron to form graphite and/or cementite. This phenomenon is referred to as carbon deposition.

In this experiment, the mass change of the hematite ore sample during reduction was considered to be caused by oxygen deprivation in the sample by hydrogen or carbon monoxide. Meanwhile, carbon deposition exists under certain experimental conditions. Therefore, the apparent reaction extent, X, of hematite was defined as the ratio of the mass change of hematite at time t to the mass of oxygen in the hematite in the original sample.

$$X = \frac{m_i - m_t}{m_o} \tag{1}$$

where m_i, m_t, and m_o are the initial sample mass, the sample mass at time t, and the oxygen mass of hematite in the original sample, respectively.

3. Results and discussion

3.1. Results

The experiments were initially performed at 1023 K, the minimum temperature examined in this work. The results are presented in Fig. 4. In the initial stage of hematite reduction, the reduction product was magnetite or wustite. As shown in Fig. 5, the experimental conditions led to this reaction, regardless of whether carbon monoxide or hydrogen was used as the reducing agent. The reduction rate and reducing gas composition in this part ($Fe_2O_3 \rightarrow Fe_3O_4 \rightarrow FeO$) did not exhibit an obvious relationship. However, in the subsequent stage of hematite reduction (FeO→Fe), the reaction produced sintered metallic iron, resulting in the deterioration of the kinetic and thermodynamic conditions. The reduction rate increased with the hydrogen content from 0vol% to 80vol%.

As the reaction continued, it generated a large amount of iron that was continuously sintered and densified. Moreover, carbon monoxide was converted to carbon in the presence of iron. When carbon was generated in the late stages of the reaction and diffused to the surface of iron–iron oxides, it reacted to form gaseous substances until the pressure reached the critical value [15]. At this point, the dense iron broke, exposing the fresh surface of the reaction sample to continue the reaction. Owing to the low bonding properties of carbon and iron carbide, the iron produced by using a reducing gas with a high carbon monoxide content was less dense. Thus, the reduction rate of pure hydrogen was not the fastest in the later stage of the reduction.

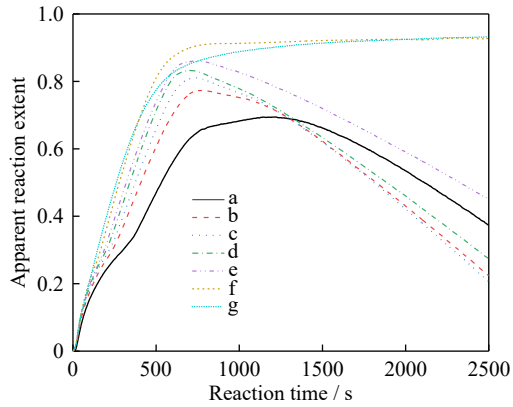

Fig. 4. Reduction degree curves for hematite with H_2/CO gas mixture at 1023 K: (a) 0vol%H_2/100vol%CO, (b) 10vol%H_2/90vol%CO, (c) 20vol%H_2/80vol%CO, (d) 35vol%H_2/65vol%CO, (e) 50vol%H_2/50vol%CO, (f) 80vol%H_2/20vol%CO, and (g) 100vol%H_2/0vol%CO.

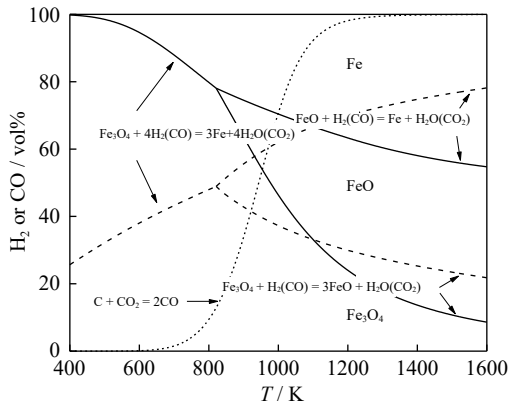

Fig. 5. Phase diagram for iron oxide reduction and Boudourad reaction (calculated with FactSage7.0).

Figs. 6 and 7 show the reduction results of the samples at 1173 and 1373 K. The reduction rate at 1173 and 1373 K was significantly higher than that at 1023 K and increased with the hydrogen content. Adding hydrogen to pure carbon monoxide gas caused the reduction rate to increase rapidly may be due to two reasons. First, the mass transfer conditions are superior because hydrogen molecules are smaller than carbon monoxide molecules. Second, the chemical driving force for the reduction of hydrogen under high-temperature conditions is greater than that of carbon monoxide.

Fig. 8 presents the XRD spectra of reaction products at 1023–1373 K. As shown in Fig. 8(a), graphite or cementite is present in the reduction product that was generated using a reducing gas containing carbon monoxide. When the carbon monoxide content was decreased to 20vol%, the graphite in the reaction product disappeared, and the content of cementite decreased to almost an undetectable level. Fig. 8(b) reflects the reaction products at 1173 K. The reaction product

with 90vol% carbon monoxide contains graphite, but the 100vol% carbon monoxide does not. With a further increase in reaction temperature and decrease in carbon monoxide content, the reaction products no longer contain graphite and cementite.

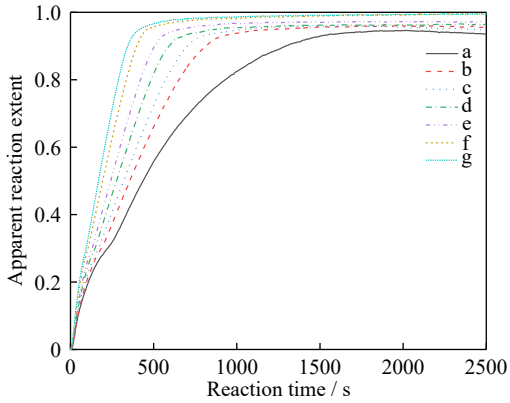

Fig. 6. Reduction degree curves for hematite with H_2/CO gas mixture at 1173 K: (a) 0vol%H_2/100vol%CO, (b) 10vol%H_2/90vol%CO, (c) 20vol%H_2/80vol%CO, (d) 35vol%H_2/65vol%CO, (e) 50vol%H_2/50vol%CO, (f) 80vol%H_2/20vol%CO, and (g) 100vol%H_2/0vol%CO.

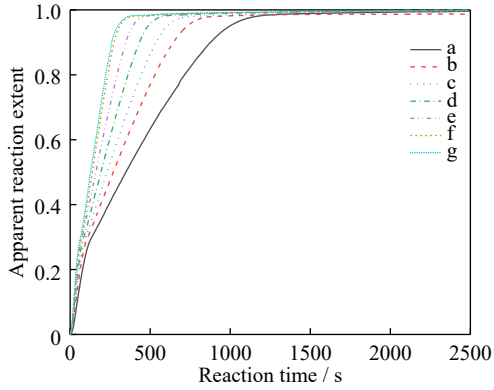

Fig. 7. Reduction degree curves for hematite with H_2/CO gas mixture at 1373 K: (a) 0vol%H_2/100vol%CO, (b) 10vol%H_2/90vol%CO, (c) 20vol%H_2/80vol%CO, (d) 35vol%H_2/65vol%CO, (e) 50vol%H_2/50vol%CO, (f) 80vol%H_2/20vol%CO, and (g) 100vol%H_2/0vol%CO.

3.2. Reduction rate

During reduction, the oxygen content in the sample generally showed an unstable trend of a rapid and then slow decrease. Hence, the whole reduction process was divided into two parts that proceeded in series for further investigation. The magnetite formed by hematite reduction was immediately reduced to wustite (part 1), which was then reduced to iron (part 2). This phenomenon was also suggested by the initial steep slope in Figs. 4, 6, and 7. The apparent reaction rates (v) were further obtained and are shown in Fig. 9. At a given temperature, the local minimum rate was achieved near the apparent reaction extent at 0.3, which indicated that the reduction began to enter the stage from wustite to iron and that a transition of reaction mechanism possibly occurred after the initial stage of reduction. At the beginning of the

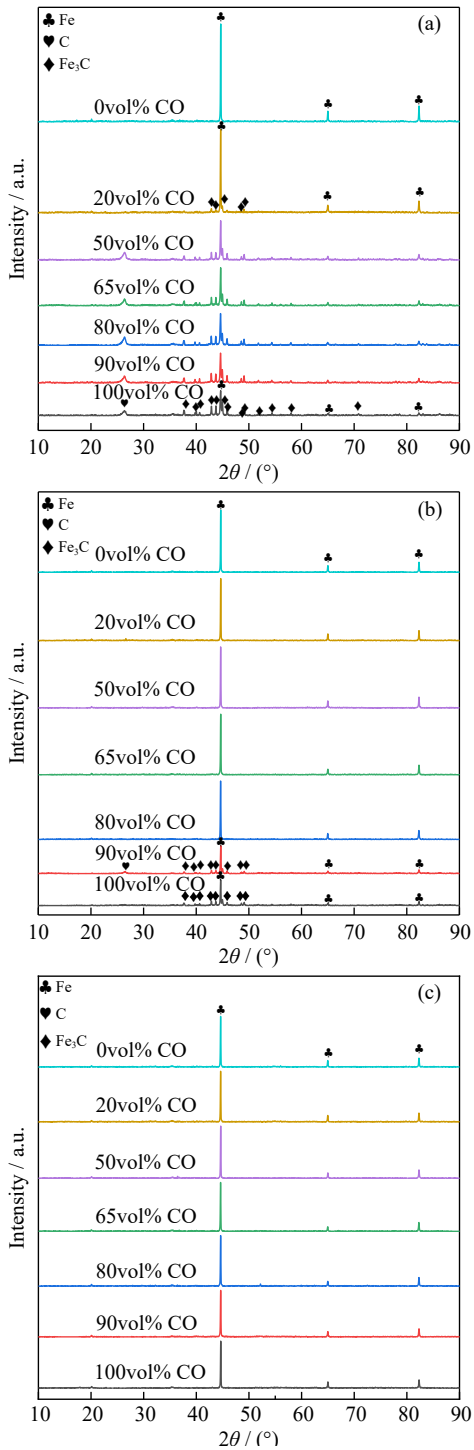

Fig. 8. XRD patterns of the reaction products at different temperatures: (a) 1023 K; (b) 1173 K; (c) 1373 K.

transition stage from wustite to iron, the iron nuclei were first formed on wustite surfaces; this phenomenon might be the main reason for the apparent rate reduction.

According to the Jacobs single-step nucleation assumption [16–17] that nucleation and nuclei growth occur in a single step, the rate of nucleation can be derived using the following equation:

$$v_t = \frac{\mathrm{d}N}{\mathrm{d}t} = K_{\mathrm{N}}(N_0 - N) \qquad (2)$$

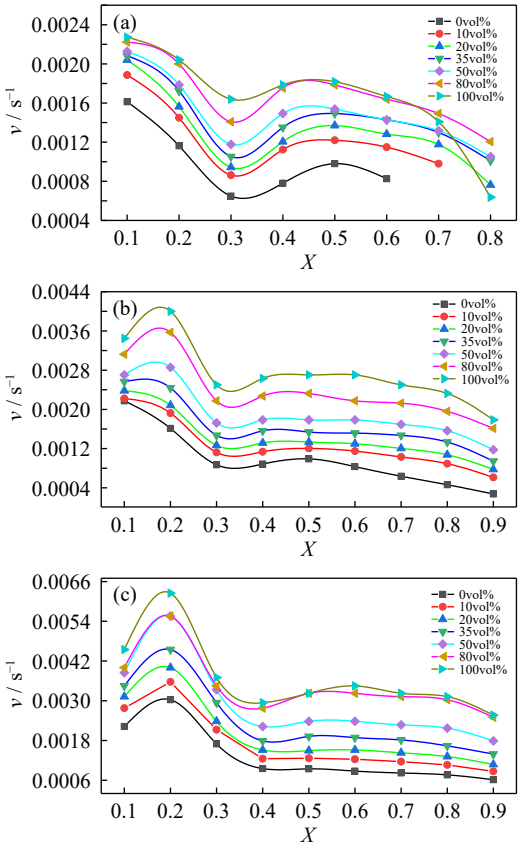

Fig. 9. Apparent reduction rate versus apparent reaction extent under different conditions: (a) 1023 K; (b) 1173 K; (c) 1373 K.

where v_t, N, N_0, and K_N are the nucleation rate at time t, the number of growth nuclei present at time t, the potential nucleation sites (having equal nucleation probability), and the nucleation rate constant, respectively. Separating the variables and integrating Eq. (2) yielded the following:

$$N = N_0\left(1 - e^{-K_N t}\right) \tag{3}$$

Substituting Eq. (3) into Eq. (2) can be shown as follows:

$$v_t = K_N N_0 e^{-K_N t} \tag{4}$$

The average rate can be expressed as follows:

$$v = \frac{\int_0^{t_a} v_t dt}{t_a} = \frac{\int_0^{t_a} K_N N_0 e^{-K_N t} dt}{t_a} \tag{5}$$

where K_N, v, and t_a represent the apparent nucleation rate constant, the apparent average rate, and the time of nucleation and growth, respectively. According to the average rate given in Fig. 9, K_N is small, and the exponential term in Eq. (4) is about 1. Hence, the equation of the average rate was simplified as follows:

$$\ln v = \ln \frac{\int_0^{t_a} K_N N_0 \times 1 dt}{t_a} = \ln K_N + \ln N_0 \tag{6}$$

El-Geassy and Rajakumar [18] indicated that the nucleation rate was closely related to C_{CO}. If K_N is considered a constant, then a functional relationship ($f(C_{CO})$) should occur between C_{CO} and N_0. Eq. (6) can be simplified and rewritten as

$$\ln v = A + F(C_{CO}) \tag{7}$$

where A, C_{CO}, and $F(C_{CO})$ are the constant part, the carbon monoxide content of the gas mixture, and the functional part of Eq. (7), respectively.

The corresponding relationships between the logarithm of the apparent average rate of reduction and the composition of reducing gas obtained from Fig. 9(b) and (c) are provided in Fig. 10. For the experiment at 1023 K, the apparent reaction extent at the later stage of reduction was not equal to the reduction extent due to the serious carbon deposition in the sample reduced using a gas containing carbon monoxide. Therefore, the reduction rate at this temperature cannot be analyzed without obtaining the absolute real-time reduction extent. For the reduction experiment with the hydrogen/carbon monoxide gas mixture at 1173 and 1373 K, the linear relationship between the average rate and the carbon monoxide content in the gas mixture can be represented by

$$\ln v = \ln v_{H_2} + B \cdot C_{CO} \tag{8}$$

where v, v_{H_2}, and B are the apparent average rate of reduction and the average rate of reduction of pure hydrogen, and a constant, respectively. Eq. (8) was not strictly derived using a purely mathematical model but obtained by assuming conditions combined with experimental results.

This linear relationship was invalid for the hydrogen composition = 0vol% (C_{CO} = 100vol%) due to the inapplicability of Eq. (8). Furthermore, the addition of hydrogen to carbon monoxide rapidly increased the reduction rate because hydrogen can increase the nucleation rate of iron nuclei.

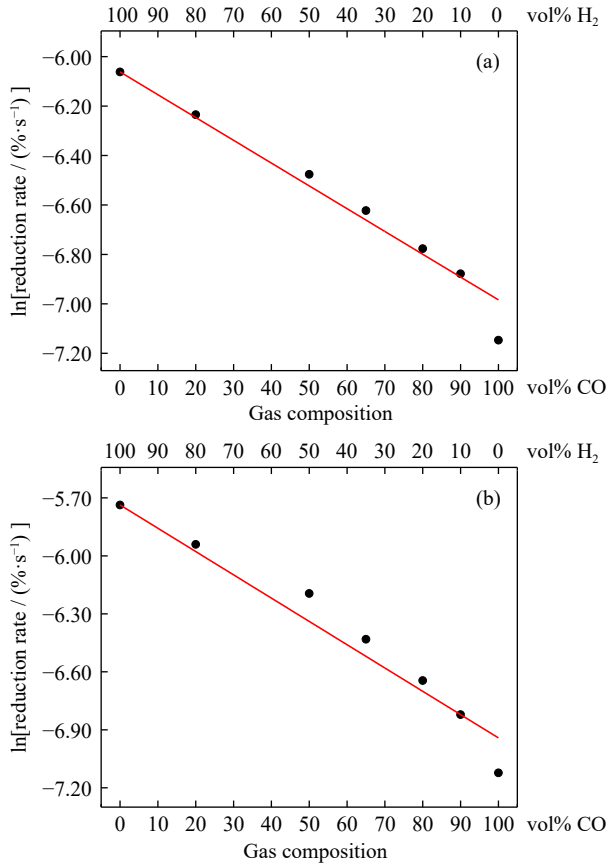

Fig. 10. Relationship between the average rate of reduction and the composition of reducing gas at (a) 1173 and (b) 1373 K.

3.3. Carbon deposition rate

With the increase in reduction temperature under the study conditions, carbon deposition was rapidly weakened. Fig. 6 shows that when the temperature was increased to 1173 K, slight carbon deposition occurred. When the temperature was increased to 1373 K, no carbon deposition was observed. Given that carbon deposition hardly occurs at high temperatures [19], the following section focuses on the obtained results (Fig. 11) at 1023 and 1173 K. The results were in good agreement with the thermodynamic simulation results calculated using FactSage software in Fig. 5.

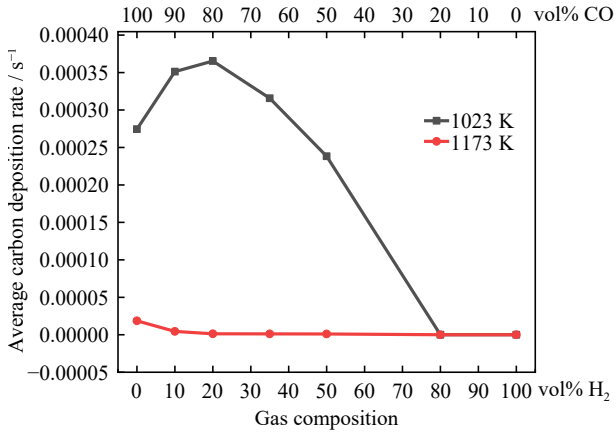

Fig. 11. Average carbon deposition rate at 1023 and 1173 K.

Carbon deposition in the hydrogen/carbon monoxide gas mixture in the presence of metallic iron can be expressed through the following steps:

① CO–CO

$$(CO)_g + \boxdot \rightleftarrows (CO)_{ads} \quad (9)$$

$$(CO)_{ads} + (CO)_g \rightarrow (CO \cdot CO)^*_{ads} \quad (10)$$

$$(CO \cdot CO)^*_{ads} \rightarrow C + (CO_2)_{ads} \quad (11)$$

$$(CO_2)_{ads} \rightarrow (CO_2)_g + \boxdot \quad (12)$$

② CO–H_2

$$(CO)_g + \boxdot \rightleftarrows (CO)_{ads} \text{ or } (H_2)_g + \boxdot \rightleftarrows (H_2)_{ads} \quad (13)$$

$$(CO)_{ads} + (H_2)_g \rightarrow (H_2 \cdot CO)^*_{ads} \text{ or } (H_2)_{ads} + (CO)_g \rightarrow (H_2 \cdot CO)^*_{ads} \quad (14)$$

$$(H_2 \cdot CO)^*_{ads} \rightarrow C + (H_2O)_{ads} \quad (15)$$

$$(H_2O)_{ads} \rightarrow (H_2O)_g + \boxdot \quad (16)$$

where $\boxdot$, $(CO \cdot CO)^*_{ads}$, and $(CO \cdot H_2)_{ads}$ are the vacant active site on metallic iron, the metastable state of carbon monoxide–carbon monoxide active molecule, and the metastable state of hydrogen–carbon monoxide active molecule, respectively.

$$3Fe + C \rightarrow Fe_3C \quad (17)$$

According to the XRD patterns, the sample that underwent carbon deposition primarily consists of iron, cementite, and graphite. The average carbon deposition rate increased with the hydrogen content until a maximum value was reached and then decreased when the hydrogen content was increased further at 1023 K. The maximum rate, which was 30% higher than that of pure carbon monoxide, was achieved when the hydrogen content was 20vol%. Metallic iron has two important roles in carbon deposition: as a reaction catalyst and a raw material for iron carbide production. With regard to the amount of iron present, the carbon deposition rate should not be the maximum when the hydrogen content was 0vol%. Fruehan [20] and Geng [21] found that the controlling step of carbon deposition reaction was the generation of $(CO \cdot CO)^*_{ads}$ and $(H_2 \cdot CO)^*_{ads}$, and the generation rate of $(H_2 \cdot CO)^*_{ads}$ was about five times faster than that of $(CO \cdot CO)^*_{ads}$. Therefore, the carbon deposition rate increased with the amount of introduced hydrogen. If the hydrogen content in the reducing gas is excessively large, then the carbon monoxide content as the main reactant of carbon deposition becomes inevitably low, thus seriously reducing the carbon deposition rate. In addition, the excessive hydrogen content in the reducing gas led to the serious sintering of the produced iron, which in turn led to a decrease in the area and rate of carbon deposition. Therefore, the carbon deposition rate increased with the hydrogen content in the reducing gas. The maximum carbon deposition rate was reached when hydrogen content was about 20vol% and then decreased when the hydrogen content was further increased. High-resolution SEM images (Fig. 12) confirmed that when the hydrogen content was lower than 50vol%, many flocculent substances appeared on the product surface. Although energy dispersive spectroscopy (EDS) produces errors in measuring light elements, the flocculent substances were analyzed using EDS to confirm their composition, as shown in Table 2.

3.4. Analysis of activation energy

The apparent activation energy (E_a) of the reaction is of great significance in understanding the rate-limiting steps and the difficulty of the reaction. Therefore, the E_a of the reaction was obtained using some methods.

$$k = A_0 e^{\frac{-E_a}{RT}} \quad (18)$$

$$\ln k = \ln\left(A_0 e^{\frac{-E_a}{RT}}\right) = \ln A_0 - \frac{E_a}{RT} \quad (19)$$

where k, A_0, and R are the rate constant of reaction, the pre-exponential (frequency) factor, and the gas constant, respectively.

$$\frac{dX}{dt} = A_0 e^{\frac{-E_a}{RT}} \cdot f(X) \quad (20)$$

$$F(X) = \int_0^X \frac{dX}{f(X)} \quad (21)$$

where $f(X)$ and $F(X)$ are the reaction mechanism model function and the integral reaction model, respectively. Separating variables and integrating Eq. (20) yielded the integral form of the isothermal rate law as follows:

$$F(X) = A_0 e^{\frac{-E_a}{RT}} \cdot t = kt \quad (22)$$

Kinetic analysis can be performed by either model-fitting or model-free method; both have their own superiority [22–24]. However, a kinetic model is usually needed for the

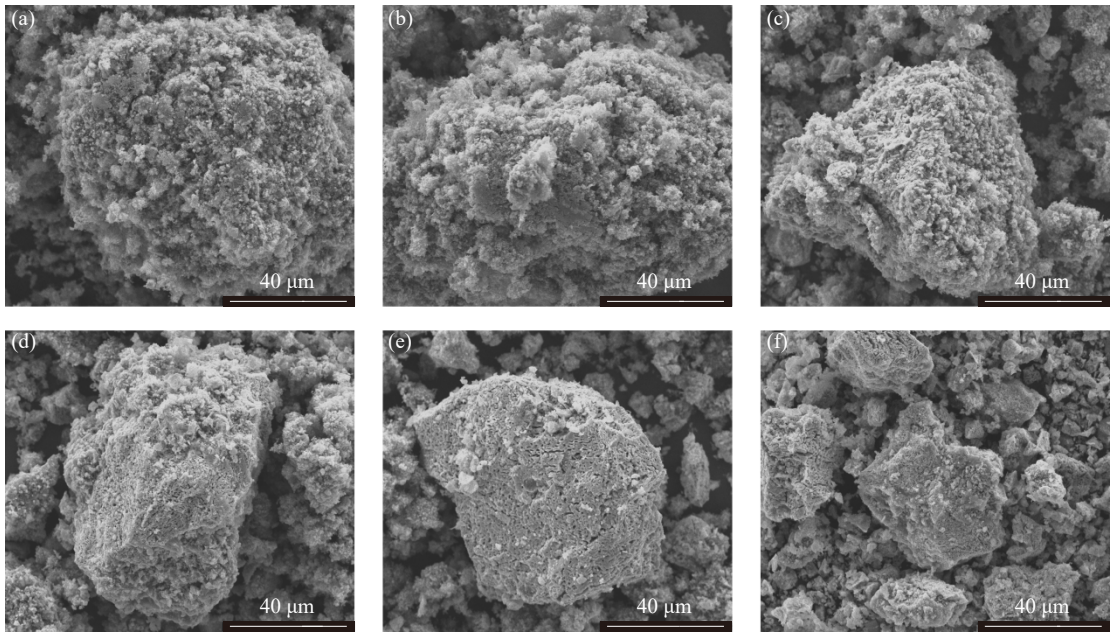

Fig. 12. High-resolution SEM images of reduction product at 1023 K: (a) 0vol%H_2/100vol%CO, (b) 10vol%H_2/90vol%CO, (c) 20vol%H_2/80vol%CO, (d) 35vol%H_2/65vol%CO, (e) 50vol%H_2/50vol%CO, and (f) 80vol%H_2/20vol%CO.

Table 2. Composition of flocculent substance analyzed by EDS

wt%

C	Fe	O	Si	Al
68.29	25.16	2.31	0.57	0.71

complete kinetic description of the solid-state reaction [25]. Hence, the model-fitting method is more accurate and comprehensive than the model-free method. Table 3 presents the suggested kinetic model functions containing integral and differential forms [17,26–28].

The apparent activation energy depends on the raw material and the physical state and purity of the reaction. Even when the reaction material is the same, any change in experimental conditions will lead to different values of apparent activation energy. According to the best fitting equation, the values of apparent activation energy of the first stage under the different reaction conditions of the gas component are shown in Fig. 13. When the hydrogen content in the reducing gas mixture was less than 20vol%, the apparent activation energy of the reaction was about 34.0 kJ/mol and remained basically unchanged. Meanwhile, when the hydrogen content was higher than 20vol%, the apparent activation energy started to increase linearly with the hydrogen content. Nonetheless, the maximum value of apparent activation energy was only 45.4 kJ/mol.

Table 3. Reaction kinetic model function applied for the solid-state reaction

Model	Integral form, $F(X)=\int_0^X \frac{dX}{f(X)}$	Differential form, $f(X)=\frac{dX/dt}{k}$
One-dimensional diffusion (D1)	X^2	$\frac{1}{2X}$
Two-dimensional diffusion (D2)	$(1-X)\ln(1-X)+X$	$-\frac{1}{\ln(1-X)}$
Three-dimensional diffusion (Jander)	$[1-(1-X)^{\frac{1}{3}}]^2$	$\frac{3(1-X)^{\frac{2}{3}}}{2[1-(1-X)^{\frac{1}{3}}]}$
Three-dimensional diffusion (Ginstling–Brounshtein)	$1-\frac{2X}{3}-(1-X)^{\frac{2}{3}}$	$\frac{3}{2[(1-X)^{-\frac{1}{3}}-1]}$
Zero-order (F0/R1)	X	1
First-order (F1)	$-\ln(1-X)$	$1-X$
Second-order (F2)	$\frac{1}{1-X}-1$	$(1-X)^2$
Contracting area (R2)	$1-(1-X)^{\frac{1}{2}}$	$2(1-X)^{\frac{1}{2}}$
Contracting volume (R3)	$1-(1-X)^{\frac{1}{3}}$	$3(1-X)^{\frac{1}{3}}$
Avrami–Erofeyev (A2)	$[-\ln(1-X)]^{\frac{1}{2}}$	$2(1-X)[-\ln(1-X)]^{\frac{1}{2}}$
Avrami–Erofeyev (A3)	$[-\ln(1-X)]^{\frac{1}{3}}$	$3(1-X)[-\ln(1-X)]^{\frac{2}{3}}$
Avrami–Erofeyev (A4)	$[-\ln(1-X)]^{\frac{1}{4}}$	$4(1-X)[-\ln(1-X)]^{\frac{3}{4}}$

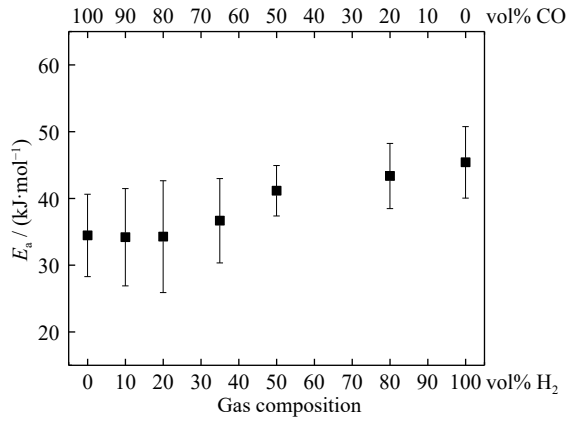

Fig. 13. Relation between the composition of reducing gas and the activation energy of reduction.

According to a previous study on the relationship between apparent activation energy and the rate-controlling step in Table 4 [29], the possible rate-controlling step is the combined gas diffusion and interfacial chemical reaction. When the hydrogen content increased, the reduction shifted toward a controlled interfacial chemical reaction. Moreover, the values of the apparent activation energy and the corresponding rate-controlling step are not decisive but rather indicative.

Table 4. Relationship between apparent activation energy and possible rate-controlling step

No.	Apparent activation energy, E_a / (kJ·mol^{-1})	Possible rate-controlling step
1	8–16	Gas diffusion
2	29–42	Combined gas diffusion and interfacial chemical reaction
3	60–67	Interfacial chemical reaction
4	>90	Solid-state diffusion

4. Conclusions

The hematite ore reduction by the hydrogen/carbon monoxide gas mixture was investigated in an accurate TGA in the temperature range of 1023–1373 K. On the basis of the results from a series of comprehensive analyses and comparisons with previous articles, the following conclusions can be drawn.

(1) The gas composition of the reducing gas mixture had the least influence on the initial part of the reduction. However, this influence increased with the reaction temperature. Hydrogen could significantly increase the reduction rate of hematite ore. The reduction rate with pure hydrogen was about three and four times higher than that with pure carbon monoxide at 1173 and 1373 K, respectively. In addition, the logarithm of the average rate was linear to the composition of the gas mixture, as shown in Eq. (8).

(2) Hydrogen could prominently promote carbon deposition under the temperature of 1023 K. When the hydrogen content in the hydrogen/carbon monoxide gas mixture was less than 20vol%, the carbon deposition rate increased with the hydrogen content. The maximum average carbon deposition rate, which was 30% higher than that of pure carbon monoxide, was reached when the hydrogen content was 20vol%.

(3) The apparent activation energy of the reduction by the hydrogen/carbon monoxide gas mixture increased from about 35.0 to 45.4 kJ/mol when the hydrogen content was increased from 20vol% to 100vol%. Therefore, the possible rate-controlling step of this reaction stage was the combined gas diffusion and interfacial chemical reaction. With the increase in the hydrogen content, the reduction became a controlled interfacial chemical reaction.

Acknowledgements

The authors were very grateful for the financial support provided by Tata Steel Limited and State Key Laboratory of Advanced Metallurgy (USTB).

Conflict of Interest

The authors declare no potential conflict of interest.

References

[1] M.C. Xie, G. Zhao, J.W. Chen, and K.L. Cao, Analysis of industrial metabolic flux in blast furnace ironmaking system, *IOP Conf. Ser.: Earth Environ. Sci.*, 358(2019), No. 3, art. No. 032034.

[2] Y. Kawashiri, T. Nouchi, and H. Matsuno, Effect of nitrogen-less reducing atmosphere on permeability of cohesive layer in blast furnace, *Tetsu-to-Hagane*, 104(2018), No. 9, p. 467.

[3] J. Tang, M.S. Chu, F. Li, C. Feng, Z.G. Liu, and Y.S. Zhou, Development and progress on hydrogen metallurgy, *Int. J. Miner. Metall. Mater.*, 27(2020), No. 6, p. 713.

[4] W.H. Kim, S. Lee, S.M. Kim, and D.J. Min, The retardation kinetics of magnetite reduction using H_2 and H_2–H_2O mixtures, *Int. J. Hydrog. Energy*, 38(2013), No. 10, p. 4194.

[5] J. Dang, Y.J. Wu, Z.P. Lv, Z.X. You, S.F. Zhang, and X.W. Lv, A new kinetic model for hydrogen reduction of metal oxides under external gas diffusion controlling condition, *Int. J. Refract. Met. Hard Mater.*, 77(2018), p. 90.

[6] R. Zhang, J. Dang, D. Liu, Z.P. Lv, G.Q. Fan, and L.W. Hu, Reduction of perovskite-geikielite by methane-hydrogen gas mixture: Thermodynamic analysis and experimental results, *Sci. Total Environ.*, 699(2020), art. No. 134355.

[7] A.A. El-Geassy and V. Rajakumar, Influence of particle size on the gaseous reduction of wustite at 900−1100°C, *ISIJ Int.*, 25(1985), No. 12, p. 1202.

[8] M.M. Sun, J.L. Zhang, K.J. Li, K. Guo, Z.M. Wang, and C.H. Jiang, Gasification kinetics of bulk coke in the CO_2/CO/H_2/H_2O/N_2 system simulating the atmosphere in the industrial blast furnace, *Int. J. Miner. Metall. Mater.*, 26(2019), No. 10, p. 1247.

[9] M.N.A. Tahari, F. Salleh, T.S.T. Saharuddin, *et al.*, Influence of hydrogen and various carbon monoxide concentrations on reduction behavior of iron oxide at low temperature, *Int. J. Hydrog. Energy*, 44(2019), No. 37, p. 20751.

[10] R.A.D. Rodriguez, A.N. Conejo, and E.B. Bedolla, Kinetics of reduction of Fe_2O_3 particles with H_2–CO mixtures at low temperatures, *Iron & Steelmaker*, 30(2003), No. 1, p. 25.

[11] A. Bonalde, A. Henriquez, and M. Manrique, Kinetic analysis

of the iron oxide reduction using hydrogen-carbon monoxide mixtures as reducing agent, *ISIJ Int.*, 45(2005), No. 9, p. 1255.
[12] A. Steinfeld, A. Frei, and P. Kuhn, Thermoanalysis of the combined Fe_3O_4-reduction and CH_4-reforming processes, *Metall. Mater. Trans. B*, 26(1995), No. 3, p. 509.
[13] N. Towhidi and J. Szekely, The influence of carbon deposition on the reduction kinetics of commercial grade hematite pellets with CO, H_2, and N_2, *Metall. Trans. B*, 14(1983), No. 3, p. 359.
[14] P. Garg, X.J. Hu, Y. Li, K.J. Li, S. Nag, and J.L. Zhang, Kinetics of iron oxide reduction in H_2/H_2O gas mixture: Global and stepwise reduction, *Metall. Mater. Trans. B*, 53(2022), No. 3, p. 1759.
[15] A.A. El-Geassy and M.I. Nasr, Influence of original structure on the kinetics and mechanisms of carbon monoxide reduction of hematite compacts, *ISIJ Int.*, 30(1990), No. 6, p. 417.
[16] W.E. Garner, *Chemistry of the Solid State*, Academic Press, New York, 1955.
[17] A. Khawam and D.R. Flanagan, Solid-state kinetic models: Basics and mathematical fundamentals, *J. Phys. Chem. B*, 110(2006), No. 35, p. 17315.
[18] A.A. El-Geassy and V. Rajakumar, Gaseous reduction of wustite with H_2, CO and H_2–CO mixtures, *ISIJ Int.*, 25(1985), No. 6, p. 449.
[19] X.J. Zuo, J.S. Wang, X.W. An, X.F. She, and Q.G. Xue, Reduction behaviors of pellets under different reducing potentials, *J. Iron Steel Res. Int.*, 20(2013), No. 12, p. 12.
[20] R.J. Fruehan, The rate of carburization of iron in CO–H_2 atmospheres: Part I. Effect of temperature and CO and H_2-pressures, *Metall. Trans.*, 4(1973), No. 9, p. 2123.
[21] S.H. Geng, *Fundamental Research on Gas-based Direct Reduction of Iron Ore with Reformed Coke Oven Gas* [Dissertation], Shanghai University, Shanghai, 2018, p. 113.
[22] A. Khawam and D.R. Flanagan, Complementary use of model-free and modelistic methods in the analysis of solid-state kinetics, *J. Phys. Chem. B*, 109(2005), No. 20, p. 10073.
[23] A.K. Galwey and M.E. Brown, Application of the Arrhenius equation to solid state kinetics: Can this be justified? *Thermochim. Acta*, 386(2002), No. 1, p. 91.
[24] A. Khawam and D.R. Flanagan, Role of isoconversional methods in varying activation energies of solid-state kinetics: I. isothermal kinetic studies, *Thermochim. Acta*, 429(2005), No. 1, p. 93.
[25] H. Tanaka, Thermal analysis and kinetics of solid state reactions, *Thermochim. Acta*, 267(1995), p. 29.
[26] A. Ortega, The kinetics of solid-state reactions toward consensus—Part I: Uncertainties, failures, and successes of conventional methods, *Int. J. Chem. Kinet.*, 33(2001), No. 6, p. 343.
[27] B. Janković, B. Adnađević, and J. Jovanović, Application of model-fitting and model-free kinetics to the study of non-isothermal dehydration of equilibrium swollen poly (acrylic acid) hydrogel: Thermogravimetric analysis, *Thermochim. Acta*, 452(2007), No. 2, p. 106.
[28] G. Munteanu, P. Budrugeac, L. Ilieva, T. Tabakova, D. Andreeva, and E. Segal, Kinetics of temperature programmed reduction of Fe_3O_4 promoted with copper: Application of iso-conversional methods, *J. Mater. Sci.*, 38(2003), No. 9, p. 1995.
[29] M.I. Nasr, A.A. Omar, M.H. Khedr, and A.A. El-Geassy, Effect of nickel oxide doping on the kinetics and mechanism of iron oxide reduction, *ISIJ Int.*, 35(1995), No. 9, p. 1043.